

Status and plans for the instrumentation of the IceCube Surface Array Enhancement

The IceCube Collaboration

(a complete list of authors can be found at the end of the proceedings)

E-mail: shefali.shefali@kit.edu, frank.schroeder@kit.edu

The surface array of IceCube, IceTop, operates primarily as a cosmic-ray detector, as well as a veto for astrophysical neutrino searches for the IceCube in-ice instrumentation. However, the snow accumulation on top of the IceTop detectors increases the detection threshold and attenuates the measured IceTop signals. Enhancing IceTop by a hybrid array of scintillation detectors and radio antennas will lower the energy threshold for air-shower measurements, provide more efficient veto capabilities, enable more accurate cosmic-ray measurements, and improve the detector calibration by compensating for snow accumulation. After the initial commissioning period, a prototype station at the South Pole has been recording air-shower data and has successfully observed coincident events of both the scintillation detectors and the radio antennas with the IceTop array. The production and calibration of the detectors for the full planned array has been ongoing. Additionally, one station each has been installed at the Pierre Auger Observatory and the Telescope Array for further R&D of these detectors in different environmental conditions. This contribution will present the status and future plans of the hybrid detector stations for the IceCube Surface Array Enhancement.

Corresponding authors: S. Shefali^{1*}, Frank G. Schroeder^{2,3}

¹ *Institute of Experimental Particle Physics, Karlsruhe Institute of Technology (KIT), Germany*

² *Institute for Astroparticle Physics, Karlsruhe Institute of Technology (KIT), Germany*

³ *Bartol Research Institute and Dept. of Physics and Astronomy, University of Delaware, USA*

* Presenter

The 38th International Cosmic Ray Conference (ICRC2023)
26 July – 3 August, 2023
Nagoya, Japan



1. Introduction

IceTop [1], the surface array of the IceCube Neutrino Observatory [2], is a unique cosmic-ray detector, which contributes significantly to the veto against the atmospheric background for the In-Ice detector. It consists of 81 pairs of Ice-Cherenkov tanks, placed on the surface of the antarctic ice covering an area of 1 km^2 . The complementary information from the surface and the In-Ice detector allows for a range of cosmic ray studies, including mass composition, energy spectra, muon density [3] [4] etc., in the energy range of 250 TeV to EeV. Since their deployment, non-uniform snow accumulation on the IceTop tanks has resulted in an increase in the detection threshold, due to attenuation in the IceTop signals. To lower this threshold, and develop a multi-component cosmic-ray detection infrastructure, an enhancement of the surface array has been proposed [5].

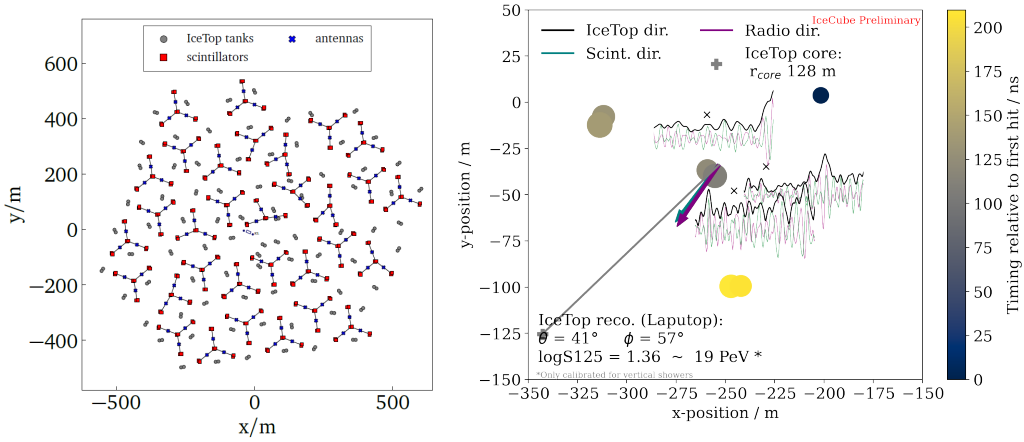


Figure 1: Left: The planned Surface Array Enhancement within the IceTop footprint; Right: An example event with 3-fold coincidence observed by IceTop, scintillation and radio detectors.

The enhancement is planned as a hybrid detector array, consisting of 32 stations within the footprint of IceTop (Fig. 1 (left)). Each station will comprise 8 scintillation detectors, 3 radio detectors and a central fieldhub data acquisition (DAQ) system. Following the intermediate R&D deployments, a fully functional prototype station was operational at the South Pole from January 2020 to December 2022. With the air-shower measurements from the prototype station alone, 3-fold coincident events with the IceTop array were already reconstructed [6]. An example of such an event is presented in Fig. 1 (right). Events coincidentally observed within $2 \mu\text{s}$ by all 3 detectors are considered to be a single coincident event. The timestamp of the first scintillation detector hit is taken as the reference time for the coincidence for the scintillator channel, while for the radio detection their trigger time is used. For the IceTop data the timestamp corresponds to when the shower is expected to hit the surface.

Efforts to significantly improve the isolation of the radio emission of the air showers from that of the Galactic and extragalactic background noise, using machine learning methods called convolution neural networks, are ongoing [7]. A successful implementation on a 2 month data set from the prototype station has been achieved. The method is able to successfully distinguish and denoise the air-shower signals, and is found to be in agreement with the traditional IceTop reconstruction. Furthermore, the X_{max} analysis of the air showers, which can be used to facilitate mass composition studies, using this data set is also in progress. Preliminary results can be found in [8].

Succeeding the prototype station, the first enhancement station has been deployed at the South Pole in January 2023. Moreover, the production of 1/4th of the planned enhancement stations has been completed. This contribution will present the deployment and commissioning of the new station, as well as the status and plans for the mass production of the proposed stations for future deployments.

2. Station 0

The most recent deployment for the Surface Array Enhancement was in January 2023. This deployment included an exchange of the 8 scintillation detectors of the existing prototype station, and one of the radio antennas. The newly installed scintillation detectors are equipped with an updated version of the readout electronic (uDAQ) board [9], which was modified to increase the dynamic range of the detectors. Additionally, a mechanical improvement in the detector casing by gluing the edges (in addition to riveting), was introduced to make the panels completely light tight. The new antenna was installed on the custom mount [10], with a pre-calibrated low noise amplifier (LNA). The remaining two antennas were already placed on the mounts in previous deployments. This resulted in the first station of the surface enhancement, *station 0*. Additionally, to avoid the snow accumulation in the coming years, the scintillation detectors, as well as the fieldhub, were raised to ≈ 1.5 m height. Fig. 2 shows the deployment of the antenna and one of the new panels.

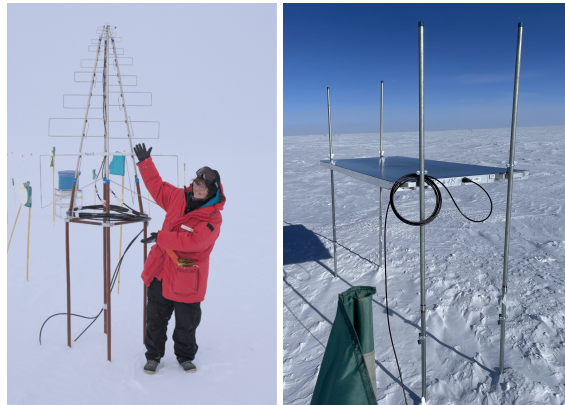


Figure 2: Left: The new deployed antenna with the custom mount; Right: One of the new scintillation detectors.

Following the deployment, a commissioning period ensued, which was used for calibration of the updated scintillation detectors. No additional calibration was required for the swapped antenna since the new antenna electronics were pre-calibrated and do not exhibit much variation with temperature [10].

Fig. 3 shows an example charge histogram of a single calibration measurement for all the 8 scintillation detectors, prior to the calibration. Along with proof of functionality, an agreement in behavior is evident for all the scintillation detectors. Owing to this, during the commissioning period, daily air-shower measurement runs were continued, along with calibration runs. For these air-shower measurements, the scintillator threshold was set to the highest digital channel (≈ 3600 ADC units [11]) where the charge deposit is comparable for all detectors, and the multiplicity

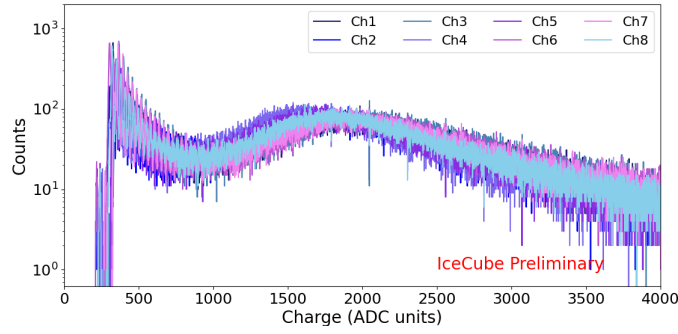


Figure 3: Charge histogram data for the 8 scintillation detectors.

for sending a trigger to the radio antennas was set to 6 or more triggered scintillation detectors. Whereas, the calibration runs included histogram measurements (in which data is histogrammed on the uDAQ board itself) at a lower threshold with a variation in the supplied bias voltage.

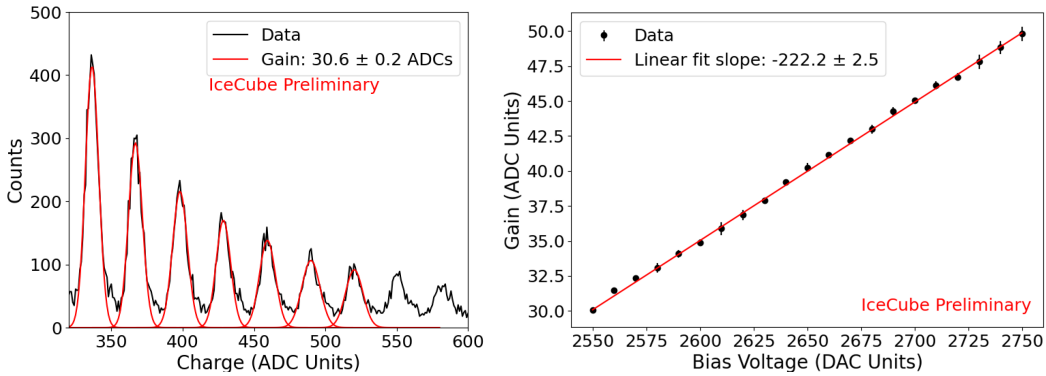


Figure 4: Features of the charge histogram data from the scintillation detectors. Left: Single Photo Electron (SPE) peaks; Right: Gain versus Bias Voltage for a single calibration run.

The charge histograms obtained from the calibration runs were further investigated, and some of the features are shown in Fig. 4. The scintillation light produced in the detectors is recorded by a Silicon Photo Multiplier (SiPM). At the low temperature environment of the South Pole (-40 to -70 °C), the gain of these SiPMs is significant, rendering the single photo electron (SPE) peaks distinguishable. These peaks can in turn be used to determine the gains of the SiPMs, and consequently stabilize it at a desired value. Fig. 4 (left) shows an example of the SPE peaks observed from a charge histogram. To identify each of the SPE peaks, a Gaussian fit is applied, and the distance between the peaks is deduced to determine the gain of the SiPM. A gain versus bias voltage plot for a single calibration run is presented in Fig. 4 (right). This calibration data was investigated for a period of 3 months, as a function of the ambient temperature recorded by the detectors. Fig. 5 presents the gain of the detectors as a function of the ambient temperature and supplied bias voltage. This relationship is modeled by a 2-dimensional plane of the form

$$\text{Gain} = a * \text{Voltage} + b * \text{Temp} + c, \quad (1)$$

for which the best-fit parameters are: $a = -0.36$, $b = 0.1$, $c = -241.03$. This is done for all scintillation detectors, with an objective of stabilizing the gain of the SiPMs which will be implemented with the upcoming version of the data acquisition software for the uDAQ board.

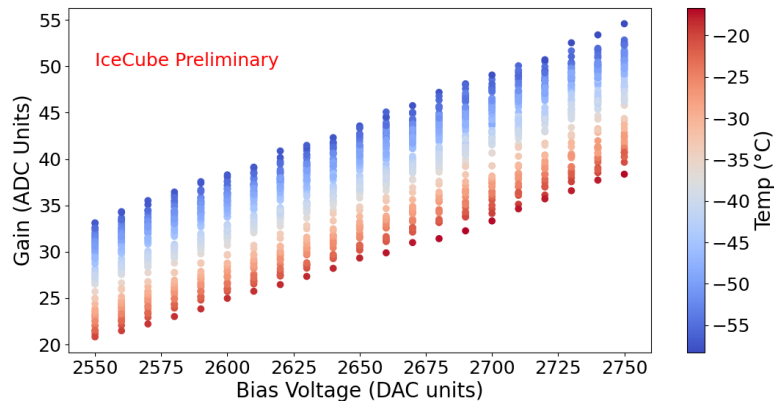


Figure 5: Gain as a function of the temperature and bias voltage from calibration data.

The light yield as well as the dynamic range of the detectors can additionally be obtained by the characterisation of the minimally ionizing particle (MIP) peak observed from the charge spectra. Example charge histograms for the three representative uDAQ gains are presented in Fig. 6. The entire charge spectrum can be described by a summation of an exponential and Landau distribution. The exponentially decaying dark noise from the SiPM is combined with the charge deposit from the MIPs, which is expected to follow a Landau distribution. This fitting is applied to the high and medium gain charge histograms. In the lowest gain, the resolution is not sufficient to resolve the two distributions, and therefore the MIP is fit with a Landau distribution only.

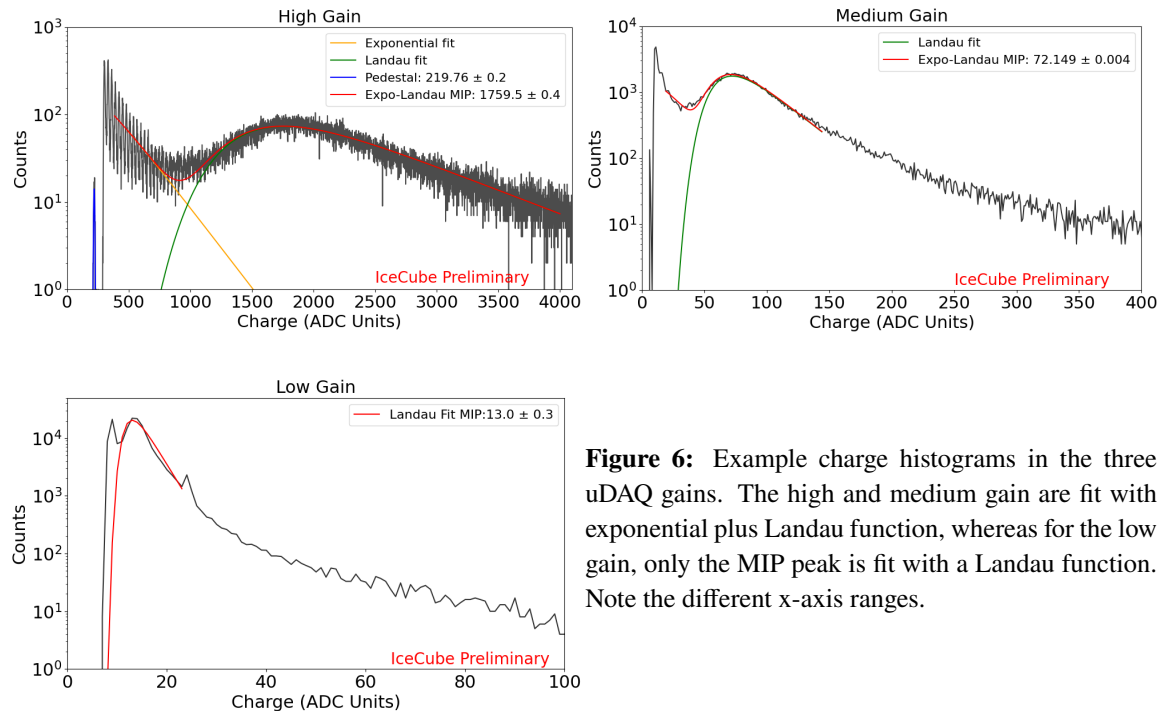


Figure 6: Example charge histograms in the three uDAQ gains. The high and medium gain are fit with exponential plus Landau function, whereas for the low gain, only the MIP peak is fit with a Landau function. Note the different x-axis ranges.

The dynamic range is determined using the ratio of the total available channels in a 12 bit ADC and the ADC units per MIP in the lowest gain. For the new detectors, this ratio implies a dynamic range of the order of ~ 800 MIPs (Fig. 6 (bottom)): The first filled bin, corresponds to the

pedestal in low gain). This is an improvement to the prototype station which had a dynamic range of 200 MIPs [11]. The light yield depends on the number of photo electrons per MIP, which is for the given example ~ 55 photo-electrons/MIP. For the specified dynamic range, this renders a total light yield of $\sim 44,000$ PEs, which is within the linear regime for the SiPMs [12].

3. Mass Production

The deployment of more enhancement stations is proposed in batches of 6 stations. The production of the scintillation and radio detectors for the first phase is complete. Fig. 7 shows pictures of the radio antennas and scintillation detectors during the production phase before shipment.



Figure 7: Left: Pre-assembly of the antenna mounts; Right: Fully assembled scintillation detectors ready for calibration tests.

The radio antennas for the 6 stations are pre-assembled, labeled and packed in single station batches. The LNAs are calibrated in a laboratory setup and shipped separately. Since the scintillation detectors are fully assembled before dispatch they have to be calibrated on the production site. Each scintillator is calibrated in a lead shielding setup [13]. The calibration measurements include:

- Coincidence measurements to send a trigger to the radio antennas, with scintillator multiplicity set from 1 up to 8 scintillation detectors
- Charge histogram measurements in the two available measurement modes on the uDAQ namely, histogram and hitbuffer, explained in [11]
- Threshold scans over the entire threshold range of the uDAQ in digital channel units.

These measurements are used to ensure the functionality of each of the produced scintillation detectors, as well as to calibrate the MIP positions at room temperatures. The room temperature measurements are carried out in a group of 8 scintillators, stacked on top of each other. Due to the high background (originating from natural radioactivity), despite a carefully chosen test setup [13], the charge histograms from each of the scintillation detectors are filtered to keep entries which correspond to hits that occur within 200 ns in all of the 8 scintillation detectors. Following this, a Landau distribution is fit to the filtered events, to localise the MIP position. Fig. 8 presents the filtered charge histogram for one of the panels in high gain. Following these room-temperature calibration tests, the scintillation detectors are further shipped for low temperature tests prior to the deployment at the South Pole.

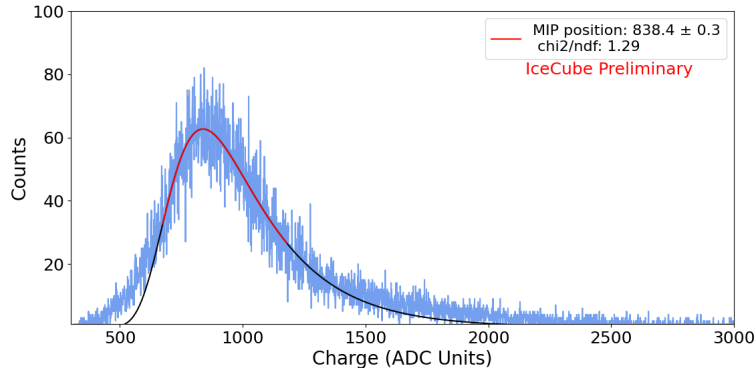


Figure 8: Charge histogram of the filtered events for one station at the production site prior to assembly, fit with a Landau function. The red curve corresponds to the region of the data where the fit is performed.

4. R&D Stations

In addition to the enhancement stations, multiple R&D stations have been produced. One full station each has been deployed at the Pierre Auger Observatory in Malargüe, Argentina and the Telescope Array (TA) in Utah, USA.

The station at the Pierre Auger Observatory has been operational since December 2022. The main aim of this station is comparing its radio measurements with the Auger Engineering Radio Array (AERA). To achieve that, the optimal trigger rate for the scintillation detectors needs to be determined, since the expected natural radioactivity from the ground, as well as the high ambient temperatures, are unfavorable for the SiPM operation. For this purpose, a threshold scan at various supplied bias voltages to the scintillation detectors is performed. Fig. 9 shows the trigger rate for the 3 different bias voltages in DAC (digital to analog convertor) units. The bias voltage is set to 3000 DAC units to achieve a nominal trigger rate at maximum threshold (~ 400 Hz), while keeping the electronic noise to a minimum. At a higher bias voltage, the electronics are expected to saturate.

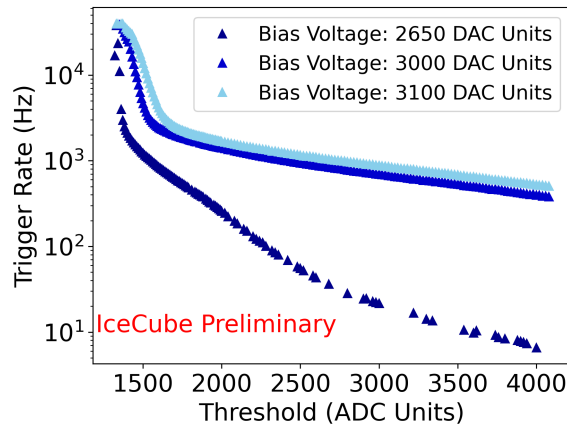


Figure 9: Threshold Scans performed at 3 varied bias voltages.

The station for the TA has been deployed in the low-energy infill region, with an objective to validate a possibility for cross calibration with the TA scintillation detectors for air shower measurements in the future for a full array [14]. Furthermore, this station will also be used for

improvement and adaptation of the central DAQ unit of the enhancement stations for the proposed next generation of the IceCube Observatory, IceCube-Gen2 [15]. This station is not yet in operation.

5. Summary

The prototype station of the Surface Array Enhancement has been taking useful R&D data at the South Pole. It has recently been upgraded, and will be the first station in the Surface Array Enhancement planned for the future. The commissioning of this station is in progress. Furthermore, promising advancements have been made for the isolation of the radio emission of air shower component from the background with the prototype station data, which will facilitate various cosmic-ray analysis. For the future deployments, 6 full stations have been produced and calibrated. Moreover, multiple developments are presented at major cosmic-ray detector sites, which will help to further improve the enhancement detectors as well as the DAQ system for IceCube-Gen2.

References

- [1] **IceCube** Collaboration *Nuclear Instruments and Methods in Physics Research Section A: Accelerators, Spectrometers, Detectors and Associated Equipment* **700** (2013) .
- [2] **IceCube** Collaboration, M. G. Aartsen *et al.* *JINST* **12** no. 03, (2017) P03012.
- [3] **IceCube** Collaboration, D. Soldin, “Cosmic Ray Measurements with IceCube and IceTop,” 8, 2022. [arXiv:2208.01911](https://arxiv.org/abs/2208.01911) [astro-ph.HE].
- [4] **IceCube** Collaboration, M. G. Aartsen *et al.* *Physical Review D* **100** no. 8, (Oct, 2019) .
- [5] **IceCube** Collaboration, A. Haungs *EPJ Web of Conferences* **210** (2019) 06009.
- [6] **IceCube** Collaboration, H. Dujmovic, A. Coleman, M. Oehler, *et al.* *PoS ICRC2021* (2021) 314.
- [7] **IceCube** Collaboration, A. Rehman, A. Coleman, and F. G. Schröder *PoS ICRC2023* (these proceedings) 291.
- [8] **IceCube** Collaboration, R. Turcotte-Tardif, S. Verpoest, and M. Venugopal *PoS ICRC2023* (these proceedings) 326.
- [9] **IceCube** Collaboration, M. Oehler, R. Turcotte-Tardif, *et al.* *PoS ICRC2021* (2021) 225.
- [10] R. Turcotte-Tardif, *Radio Measurements of Cosmic Rays at the South Pole*. PhD thesis, Karlsruhe Institut für Technologie (KIT), 2022.
- [11] M. J. Oehler, *The Prototype Station for the IceCube Surface Array Enhancement*. PhD thesis, Karlsruhe Institut für Technologie (KIT), 2022.
- [12] T. Bretz, J. Kemp, L. Middendorf, C. Peters, J. Schumacher, R. Engel, R. Smida, and D. Veberic *PoS ICRC2017* (2018) 472.
- [13] **IceCube** Collaboration, S. Shefali *PoS ECRS* (2023) 141.
- [14] N. Goehlke, “An IceCube Surface Array Enhancement station for the deployment at Telescope Array,” Master’s thesis, Karlsruhe Institut für Technologie (KIT), 2022.
- [15] **IceCube-Gen2** Collaboration, F. G. Schroeder *et al.* *PoS ICRC2021* (2021) 407.

Full Author List: IceCube Collaboration

R. Abbasi¹⁷, M. Ackermann⁶³, J. Adams¹⁸, S. K. Agarwalla^{40, 64}, J. A. Aguilar¹², M. Ahlers²², J.M. Alameddine²³, N. M. Amin⁴⁴, K. Andeen⁴², G. Anton²⁶, C. Argüelles¹⁴, Y. Ashida⁵³, S. Athanasiadou⁶³, S. N. Axani⁴⁴, X. Bai⁵⁰, A. Balagopal V.⁴⁰, M. Baricevic⁴⁰, S. W. Barwick³⁰, V. Basu⁴⁰, R. Bay⁸, J. J. Beatty^{20, 21}, J. Becker Tjus^{11, 65}, J. Beise⁶¹, C. Bellenghi²⁷, C. Benning¹, S. BenZvi⁵², D. Berley¹⁹, E. Bernardini⁴⁸, D. Z. Besson³⁶, E. Blaufuss¹⁹, S. Blot⁶³, F. Bontempo³¹, J. Y. Book¹⁴, C. Boscolo Meneguolo⁴⁸, S. Böser⁴¹, O. Botner⁶¹, J. Böttcher¹, E. Bourbeau²², J. Braun⁴⁰, B. Brinson⁶, J. Brostean-Kaiser⁶³, R. T. Burley², R. S. Busse⁴³, D. Butterfield⁴⁰, M. A. Campana⁴⁹, K. Carloni¹⁴, E. G. Carnie-Bronca², S. Chattopadhyay^{40, 64}, N. Chau¹², C. Chen⁶, Z. Chen⁵⁵, D. Chirkin⁴⁰, S. Choi⁵⁶, B. A. Clark¹⁹, L. Classen⁴³, A. Coleman⁶¹, G. H. Collin¹⁵, A. Connolly^{20, 21}, J. M. Conrad¹⁵, P. Coppin¹³, P. Correa¹³, D. F. Cowen^{59, 60}, P. Dave⁶, C. De Clercq¹³, J. J. DeLaunay⁵⁸, D. Delgado¹⁴, S. Deng¹, K. Deoskar⁵⁴, A. Desai⁴⁰, P. Desati⁴⁰, K. D. de Vries¹³, G. de Wasseige³⁷, T. DeYoung²⁴, A. Diaz¹⁵, J. C. Díaz-Vélez⁴⁰, M. Dittmer⁴³, A. Domi²⁶, H. Dujmovic⁴⁰, M. A. DuVernois⁴⁰, T. Ehrhardt⁴¹, P. Eller²⁷, E. Ellinger⁶², S. El Mentawi¹, D. Elsässer²³, R. Engel^{31, 32}, H. Erpenbeck⁴⁰, J. Evans¹⁹, P. A. Evenson⁴⁴, K. L. Fan¹⁹, K. Fang⁴⁰, K. Farrag¹⁶, A. R. Fazzari⁷, A. Fedynitch⁵⁷, N. Feigl¹⁰, S. Fiedlschuster²⁶, C. Finley⁵⁴, L. Fischer⁶⁷, D. Fox⁵⁹, A. Frankowiak¹¹, A. Fritz⁴¹, P. Fürst¹, J. Gallagher³⁹, E. Ganster¹, A. Garcia¹⁴, L. Gerhardt⁹, A. Ghadimi⁵⁸, C. Glaser⁶¹, T. Glauch²⁷, T. Glüsenkamp^{26, 61}, N. Goehke³², J. G. Gonzalez⁴⁴, S. Goswami⁵⁸, D. Grant²⁴, S. J. Gray¹⁹, O. Gries¹, S. Griffin⁴⁰, S. Griswold⁵², K. M. Groth²², C. Günther¹, P. Gutjahr²³, C. Haack²⁶, A. Hallgren⁶¹, R. Halliday²⁴, L. Halve¹, F. Halzen⁴⁰, H. Hamdaoui⁵⁵, M. Ha Minh²⁷, K. Hanson⁴⁰, J. Hardin¹⁵, A. A. Harnisch²⁴, P. Hatch³³, A. Haungs³¹, K. Helbing⁶², J. Hellrung¹¹, F. Henningsen²⁷, L. Heuermann¹, N. Heyer⁶¹, S. Hickford⁶², A. Hidvegi⁵⁴, C. Hill¹⁶, G. C. Hill², K. D. Hoffman¹⁹, S. Hori⁴⁰, K. Hoshina^{40, 66}, W. Hou³¹, T. Huber³¹, K. Hultqvist⁵⁴, M. Hünnefeld²³, R. Hussain⁴⁰, K. Hymon²³, S. In⁵⁶, A. Ishihara¹⁶, M. Jacquart¹⁶, O. Janik¹, M. Jansson⁵⁴, G. S. Japaridze⁵, M. Jeong⁵⁶, M. Jin¹⁴, B. J. P. Jones⁴, D. Kang³¹, W. Kang⁵⁶, X. Kang⁴⁹, A. Kappes⁴³, D. Kappesser⁴¹, L. Kardum²³, T. Karg⁶³, M. Karle²⁷, A. Karle⁴⁰, U. Katz²⁶, M. Kauer⁴⁰, J. L. Kelley⁴⁰, A. Khatee Zathul⁴⁰, A. Kheirandish^{34, 35}, J. Kiryluk⁵⁵, S. R. Klein^{8, 9}, A. Kochocki²⁴, R. Koirala⁴⁴, H. Kolanoski¹⁰, T. Kontrimas²⁷, L. Köpke⁴¹, C. Kopper²⁶, D. J. Koskinen²², P. Koundal³¹, M. Kovacevich⁴⁹, M. Kowalski^{10, 63}, T. Kozynets²², J. Krishnamoorthi^{40, 64}, K. Kruijswijk³⁷, E. Krupczak²⁴, A. Kumar⁶³, E. Kun¹¹, N. Kurahashi⁴⁹, N. Lad⁶³, C. Lagunas Gualda⁶³, M. Lamoureux³⁷, M. J. Larson¹⁹, S. Latseva¹, F. Lauber⁶², J. P. Lazar^{14, 40}, J. W. Lee⁵⁶, K. Leonard DeHolton⁶⁰, A. Leszczyńska⁴⁴, M. Lincetto¹¹, Q. R. Liu⁴⁰, M. Liubarska²⁵, E. Lohfink⁴¹, C. Love⁴⁹, C. J. Lozano Mariscal⁴³, L. Lu⁴⁰, F. Lucarelli²⁸, W. Luszczyk^{20, 21}, Y. Lyu^{8, 9}, J. Madsen⁴⁰, K. B. M. Mahn²⁴, Y. Makino⁴⁰, E. Manao²⁷, S. Mancina^{40, 48}, W. Marie Sainte⁴⁰, I. C. Mariş¹², S. Marka⁴⁶, Z. Marka⁴⁶, M. Marsee⁵⁸, I. Martinez-Soler¹⁴, R. Maruyama⁴⁵, F. Mayhew²⁴, T. McElroy²⁵, F. McNally³⁸, J. V. Mead²², K. Meagher⁴⁰, S. Mechbal⁶³, A. Medina²¹, M. Meier¹⁶, Y. Merckx¹³, L. Merten¹¹, J. Micallef²⁴, J. Mitchell⁷, T. Montaruli²⁸, R. W. Moore²⁵, Y. Morii¹⁶, R. Morse⁴⁰, M. Moulai⁴⁰, T. Mukherjee³¹, R. Naab⁶³, R. Nagai¹⁶, M. Nakos⁴⁰, U. Naumann⁶², J. Necker⁶³, A. Negi⁴, M. Neumann⁴³, H. Niederhausen²⁴, M. U. Nisa²⁴, A. Noell¹, A. Novikov⁴⁴, S. C. Nowicki²⁴, A. Obertacke Pollmann¹⁶, V. O'Dell⁴⁰, M. Oehler³¹, B. Oeyen²⁹, A. Olivas¹⁹, R. Ørsøe²⁷, J. Osborn⁴⁰, E. O'Sullivan⁶¹, H. Pandya⁴⁴, N. Park³³, G. K. Parker⁴, E. N. Paudel⁴⁴, L. Paul^{42, 50}, C. Pérez de los Heros⁶¹, J. Peterson⁴⁰, S. Philippen¹, A. Pizzuto⁴⁰, M. Plum⁵⁰, A. Pontén⁶¹, Y. Popovych⁴¹, M. Prado Rodriguez⁴⁰, B. Pries²⁴, R. Procter-Murphy¹⁹, G. T. Przybylski⁹, C. Raab³⁷, J. Rack-Helleis⁴¹, K. Rawlins³, Z. Rechav⁴⁰, A. Rehman⁴⁴, P. Reichherzer¹¹, G. Renzi¹², E. Resconi²⁷, S. Reusch⁶³, W. Rhode²³, B. Riedel⁴⁰, A. Rifaie¹, E. J. Roberts², S. Robertson^{8, 9}, S. Rodan⁵⁶, G. Roellinghoff⁵⁶, M. Rongen²⁶, C. Rott^{53, 56}, T. Ruhe²³, L. Ruohan²⁷, D. Ryckbosch²⁹, I. Safa^{14, 40}, J. Saffer³², D. Salazar-Gallegos²⁴, P. Sampathkumar³¹, S. E. Sanchez Herrera²⁴, A. Sandrock⁶², M. Santander⁵⁸, S. Sarkar²⁵, S. Sarkar⁴⁷, J. Savelberg¹, P. Savina⁴⁰, M. Schaufel¹, H. Schieler³¹, S. Schindler²⁶, L. Schlickmann¹, B. Schlüter⁴³, F. Schlüter¹², N. Schmeisser⁶², T. Schmidt¹⁹, J. Schneider²⁶, F. G. Schröder^{31, 44}, L. Schumacher²⁶, G. Schwefer¹, S. Sclafani¹⁹, D. Seckel⁴⁴, M. Seikh³⁶, S. Seunarine⁵¹, R. Shah⁴⁹, A. Sharma⁶¹, S. Shefali³², N. Shimizu¹⁶, M. Silva⁴⁰, B. Skrzypek¹⁴, B. Smithers⁴, R. Snihur⁴⁰, J. Soedingrekso²³, A. Sogaard²², D. Soldin³², P. Soldin¹, G. Sommani¹¹, C. Spannfellner²⁷, G. M. Spiczak⁵¹, C. Spiering⁶³, M. Stamatikos²¹, T. Stanev⁴⁴, T. Stetzelberger⁹, T. Stürwald⁶², T. Stuttard²², G. W. Sullivan¹⁹, I. Taboada⁶, S. Ter-Antonyan⁷, M. Thiesmeyer¹, W. G. Thompson¹⁴, J. Thwaites⁴⁰, S. Tilav⁴⁴, K. Tollefson²⁴, C. Tönnis⁵⁶, S. Toscano¹², D. Tosi⁴⁰, A. Trettin⁶³, C. F. Tung⁶, R. Turcotte³¹, J. P. Twagirayezu²⁴, B. Ty⁴⁰, M. A. Unland Elorrieta⁴³, A. K. Upadhyay^{40, 64}, K. Upshaw⁷, N. Valtonen-Mattila⁶¹, J. Vandenbroucke⁴⁰, N. van Eijndhoven¹³, D. Vannerom¹⁵, J. van Santen⁶³, J. Vara⁴³, J. Veitch-Michaelis⁴⁰, M. Venugopal³¹, M. Vereecken³⁷, S. Verpoest⁴⁴, D. Veske⁴⁶, A. Vijai¹⁹, C. Walck⁵⁴, C. Weaver²⁴, P. Weigel¹⁵, A. Weindl³¹, J. Weldert⁶⁰, C. Wendt⁴⁰, J. Werthebach²³, M. Weyrauch³¹, N. Whitehorn²⁴, C. H. Wiebusch¹, N. Willey²⁴, D. R. Williams⁵⁸, L. Witthaus²³, A. Wolf¹, M. Wolf²⁷, G. Wrede²⁶, X. W. Xu⁷, J. P. Yanez²⁵, E. Yildizci⁴⁰, S. Yoshida¹⁶, R. Young³⁶, F. Yu¹⁴, S. Yu²⁴, T. Yuan⁴⁰, Z. Zhang⁵⁵, P. Zhelnin¹⁴, M. Zimmerman⁴⁰

¹ III. Physikalisches Institut, RWTH Aachen University, D-52056 Aachen, Germany

² Department of Physics, University of Adelaide, Adelaide, 5005, Australia

³ Dept. of Physics and Astronomy, University of Alaska Anchorage, 3211 Providence Dr., Anchorage, AK 99508, USA

⁴ Dept. of Physics, University of Texas at Arlington, 502 Yates St., Science Hall Rm 108, Box 19059, Arlington, TX 76019, USA

⁵ CTSPS, Clark-Atlanta University, Atlanta, GA 30314, USA

⁶ School of Physics and Center for Relativistic Astrophysics, Georgia Institute of Technology, Atlanta, GA 30332, USA

⁷ Dept. of Physics, Southern University, Baton Rouge, LA 70813, USA

⁸ Dept. of Physics, University of California, Berkeley, CA 94720, USA

⁹ Lawrence Berkeley National Laboratory, Berkeley, CA 94720, USA

¹⁰ Institut für Physik, Humboldt-Universität zu Berlin, D-12489 Berlin, Germany

¹¹ Fakultät für Physik & Astronomie, Ruhr-Universität Bochum, D-44780 Bochum, Germany

¹² Université Libre de Bruxelles, Science Faculty CP230, B-1050 Brussels, Belgium

- ¹³ Vrije Universiteit Brussel (VUB), Dienst ELEM, B-1050 Brussels, Belgium
¹⁴ Department of Physics and Laboratory for Particle Physics and Cosmology, Harvard University, Cambridge, MA 02138, USA
¹⁵ Dept. of Physics, Massachusetts Institute of Technology, Cambridge, MA 02139, USA
¹⁶ Dept. of Physics and The International Center for Hadron Astrophysics, Chiba University, Chiba 263-8522, Japan
¹⁷ Department of Physics, Loyola University Chicago, Chicago, IL 60660, USA
¹⁸ Dept. of Physics and Astronomy, University of Canterbury, Private Bag 4800, Christchurch, New Zealand
¹⁹ Dept. of Physics, University of Maryland, College Park, MD 20742, USA
²⁰ Dept. of Astronomy, Ohio State University, Columbus, OH 43210, USA
²¹ Dept. of Physics and Center for Cosmology and Astro-Particle Physics, Ohio State University, Columbus, OH 43210, USA
²² Niels Bohr Institute, University of Copenhagen, DK-2100 Copenhagen, Denmark
²³ Dept. of Physics, TU Dortmund University, D-44221 Dortmund, Germany
²⁴ Dept. of Physics and Astronomy, Michigan State University, East Lansing, MI 48824, USA
²⁵ Dept. of Physics, University of Alberta, Edmonton, Alberta, Canada T6G 2E1
²⁶ Erlangen Centre for Astroparticle Physics, Friedrich-Alexander-Universität Erlangen-Nürnberg, D-91058 Erlangen, Germany
²⁷ Technical University of Munich, TUM School of Natural Sciences, Department of Physics, D-85748 Garching bei München, Germany
²⁸ Département de physique nucléaire et corpusculaire, Université de Genève, CH-1211 Genève, Switzerland
²⁹ Dept. of Physics and Astronomy, University of Gent, B-9000 Gent, Belgium
³⁰ Dept. of Physics and Astronomy, University of California, Irvine, CA 92697, USA
³¹ Karlsruhe Institute of Technology, Institute for Astroparticle Physics, D-76021 Karlsruhe, Germany
³² Karlsruhe Institute of Technology, Institute of Experimental Particle Physics, D-76021 Karlsruhe, Germany
³³ Dept. of Physics, Engineering Physics, and Astronomy, Queen's University, Kingston, ON K7L 3N6, Canada
³⁴ Department of Physics & Astronomy, University of Nevada, Las Vegas, NV, 89154, USA
³⁵ Nevada Center for Astrophysics, University of Nevada, Las Vegas, NV 89154, USA
³⁶ Dept. of Physics and Astronomy, University of Kansas, Lawrence, KS 66045, USA
³⁷ Centre for Cosmology, Particle Physics and Phenomenology - CP3, Université catholique de Louvain, Louvain-la-Neuve, Belgium
³⁸ Department of Physics, Mercer University, Macon, GA 31207-0001, USA
³⁹ Dept. of Astronomy, University of Wisconsin–Madison, Madison, WI 53706, USA
⁴⁰ Dept. of Physics and Wisconsin IceCube Particle Astrophysics Center, University of Wisconsin–Madison, Madison, WI 53706, USA
⁴¹ Institute of Physics, University of Mainz, Staudinger Weg 7, D-55099 Mainz, Germany
⁴² Department of Physics, Marquette University, Milwaukee, WI, 53201, USA
⁴³ Institut für Kernphysik, Westfälische Wilhelms-Universität Münster, D-48149 Münster, Germany
⁴⁴ Bartol Research Institute and Dept. of Physics and Astronomy, University of Delaware, Newark, DE 19716, USA
⁴⁵ Dept. of Physics, Yale University, New Haven, CT 06520, USA
⁴⁶ Columbia Astrophysics and Nevis Laboratories, Columbia University, New York, NY 10027, USA
⁴⁷ Dept. of Physics, University of Oxford, Parks Road, Oxford OX1 3PU, United Kingdom
⁴⁸ Dipartimento di Fisica e Astronomia Galileo Galilei, Università Degli Studi di Padova, 35122 Padova PD, Italy
⁴⁹ Dept. of Physics, Drexel University, 3141 Chestnut Street, Philadelphia, PA 19104, USA
⁵⁰ Physics Department, South Dakota School of Mines and Technology, Rapid City, SD 57701, USA
⁵¹ Dept. of Physics, University of Wisconsin, River Falls, WI 54022, USA
⁵² Dept. of Physics and Astronomy, University of Rochester, Rochester, NY 14627, USA
⁵³ Department of Physics and Astronomy, University of Utah, Salt Lake City, UT 84112, USA
⁵⁴ Oskar Klein Centre and Dept. of Physics, Stockholm University, SE-10691 Stockholm, Sweden
⁵⁵ Dept. of Physics and Astronomy, Stony Brook University, Stony Brook, NY 11794-3800, USA
⁵⁶ Dept. of Physics, Sungkyunkwan University, Suwon 16419, Korea
⁵⁷ Institute of Physics, Academia Sinica, Taipei, 11529, Taiwan
⁵⁸ Dept. of Physics and Astronomy, University of Alabama, Tuscaloosa, AL 35487, USA
⁵⁹ Dept. of Astronomy and Astrophysics, Pennsylvania State University, University Park, PA 16802, USA
⁶⁰ Dept. of Physics, Pennsylvania State University, University Park, PA 16802, USA
⁶¹ Dept. of Physics and Astronomy, Uppsala University, Box 516, S-75120 Uppsala, Sweden
⁶² Dept. of Physics, University of Wuppertal, D-42119 Wuppertal, Germany
⁶³ Deutsches Elektronen-Synchrotron DESY, Platanenallee 6, 15738 Zeuthen, Germany
⁶⁴ Institute of Physics, Sachivalaya Marg, Sainik School Post, Bhubaneswar 751005, India
⁶⁵ Department of Space, Earth and Environment, Chalmers University of Technology, 412 96 Gothenburg, Sweden
⁶⁶ Earthquake Research Institute, University of Tokyo, Bunkyo, Tokyo 113-0032, Japan

Acknowledgements

The authors gratefully acknowledge the support from the following agencies and institutions: USA – U.S. National Science Foundation-Office of Polar Programs, U.S. National Science Foundation-Physics Division, U.S. National Science Foundation-EPSCoR, Wisconsin Alumni Research Foundation, Center for High Throughput Computing (CHTC) at the University of Wisconsin–Madison, Open Science

Grid (OSG), Advanced Cyberinfrastructure Coordination Ecosystem: Services & Support (ACCESS), Frontera computing project at the Texas Advanced Computing Center, U.S. Department of Energy-National Energy Research Scientific Computing Center, Particle astrophysics research computing center at the University of Maryland, Institute for Cyber-Enabled Research at Michigan State University, and Astroparticle physics computational facility at Marquette University; Belgium – Funds for Scientific Research (FRS-FNRS and FWO), FWO Odysseus and Big Science programmes, and Belgian Federal Science Policy Office (Belspo); Germany – Bundesministerium für Bildung und Forschung (BMBF), Deutsche Forschungsgemeinschaft (DFG), Helmholtz Alliance for Astroparticle Physics (HAP), Initiative and Networking Fund of the Helmholtz Association, Deutsches Elektronen Synchrotron (DESY), and High Performance Computing cluster of the RWTH Aachen; Sweden – Swedish Research Council, Swedish Polar Research Secretariat, Swedish National Infrastructure for Computing (SNIC), and Knut and Alice Wallenberg Foundation; European Union – EGI Advanced Computing for research; Australia – Australian Research Council; Canada – Natural Sciences and Engineering Research Council of Canada, Calcul Québec, Compute Ontario, Canada Foundation for Innovation, WestGrid, and Compute Canada; Denmark – Villum Fonden, Carlsberg Foundation, and European Commission; New Zealand – Marsden Fund; Japan – Japan Society for Promotion of Science (JSPS) and Institute for Global Prominent Research (IGPR) of Chiba University; Korea – National Research Foundation of Korea (NRF); Switzerland – Swiss National Science Foundation (SNSF); United Kingdom – Department of Physics, University of Oxford. This project has received funding from the European Research Council (ERC) under the European Union’s Horizon 2020 research and innovation programme (grant agreement No 802729).